Title: Probing bulky ligand entry in engineered archaeal ferritins

Authors: Lorenzo Calisti, Irene Benni, Matilde Cardoso Trabuco, Paola Baiocco, Barbara Ruzicka, Alberto Boffi, Elisabetta Falvo, Francesco Malatesta, Alessandra Bonamore

Year: 2016
DOI: 10.1016/j.bbagen.2016.10.007

DOI: 10.5281/zenodo.2528583

Probing bulky ligand entry in engineered archaeal ferritins

Lorenzo Calisti, Irene Benni, Matilde Cardoso Trabuco, Paola Baiocco, Barbara Ruzicka, Alberto Boffi, Elisabetta Falvo, Francesco Malatesta, Alessandra Bonamore

PII: S0304-4165(16)30381-6
DOI: doi:10.1016/j.bbagen.2016.10.007
Reference: BBAGEN 28633

To appear in: *BBA - General Subjects*

Received date: 31 May 2016
Revised date: 1 September 2016
Accepted date: 11 October 2016

Please cite this article as: Lorenzo Calisti, Irene Benni, Matilde Cardoso Trabuco, Paola Baiocco, Barbara Ruzicka, Alberto Boffi, Elisabetta Falvo, Francesco Malatesta, Alessandra Bonamore, Probing bulky ligand entry in engineered archaeal ferritins, *BBA - General Subjects* (2016), doi:10.1016/j.bbagen.2016.10.007

Title: Probing bulky ligand entry in engineered archaeal ferritins

Authors: Lorenzo Calisti, Irene Benni, Matilde Cardoso Trabuco, Paola Baiocco, Barbara Ruzicka, Alberto Boffi, Elisabetta Falvo, Francesco Malatesta, Alessandra Bonamore

Year: 2016
DOI: 10.1016/j.bbagen.2016.10.007

DOI: 10.5281/zenodo.2528583

PROBING BULKY LIGAND ENTRY IN ENGINEERED ARCHAEAL FERRITINS.

Lorenzo Calisti[a], Irene Benni[a], Matilde Cardoso Trabuco[a], Paola Baiocco[b], Barbara Ruzicka[c], Alberto Boffi[a,d], Elisabetta Falvo[d], Francesco Malatesta[a] and Alessandra Bonamore[a].

a. Department of Biochemical Sciences "Alessandro Rossi Fanelli", Sapienza University of Rome, P.le Aldo Moro 5, I-00185 Rome, Italy.
b. Center for Life Nano Science@Sapienza, Istituto Italiano di Tecnologia, V.le Regina Elena 291, Rome I-00185, Italy.
c. Istituto dei Sistemi Complessi del Consiglio Nazionale delle Ricerche (ISC-CNR) Sede Sapienza and Dipartimento di Fisica, Sapienza University of Rome, P.le Aldo Moro 5, I-00185 Rome, Italy.
d. Istituto di Biologia e Patologia Molecolari, Consiglio Nazionale delle Ricerche (IBPM-CNR) Sede Sapienza University of Rome, P.le Aldo Moro 5, I-00185 Rome, Italy.

Keywords: Self-Assembly, Binding kinetics, Nano-scaffold, Ferritin.

ABSTRACT

Background

A set of engineered ferritin mutants from *Archaeoglobus fulgidus* (Af-Ft) and *Pyrococcus furiosus* (Pf-Ft) bearing cysteine thiols in selected topological positions inside or outside the ferritin shell have been obtained. The two apo-proteins were taken as model systems for ferritin internal cavity accessibility in that Af-Ft is characterized by the presence of a 45 Å wide aperture on the protein surface whereas Pf-Ft displays canonical (threefold) channels.

Methods

Thiol reactivity has been probed in kinetic experiments in order to assess the protein matrix permeation properties towards the bulky thiol reactive DTNB (5,5'-dithiobis-2-nitrobenzoic acid) molecule.

Results

Reaction of DTNB with thiols was observed in all ferritin mutants, including those bearing free cysteine thiols inside the ferritin cavity. As expected, a ferritin mutant from Pf-Ft, in which the cysteine thiol is on the outer surface displays the fastest binding kinetics. In turn, also the Pf-Ft mutant in which the cysteine thiol is placed within the internal cavity, is still capable of full stoichiometric DTNB binding albeit with an almost 200-fold slower rate. The behaviour of Af-Ft bearing a cysteine thiol in a topologically equivalent position in the internal cavity was intermediate among the two Pf-Ft mutants.

Conclusions and General Significance

The data thus obtained indicate clearly that the protein matrix in archaea ferritins does not provide a significant barrier against bulky, negatively charged ligands such as DTNB, a finding of relevance in view of the multiple biotechnological applications of these ferritins that envisage ligand encapsulation within the internal cavity.

1. INTRODUCTION

Ferritins from a variety of species have emerged as versatile scaffolds for a number of diverse nanotechnological applications spanning from the synthesis of metal nanoparticles to drugs or diagnostics delivery. The most notable property of ferritins resides in their ability to sequester metals as well as small molecules within their internal cavities. Ferritin proteins are by far the best-studied biomineralisation scaffolds in that these proteins are able to accommodate up to 4500 iron atoms in an iron (III) oxide form within the central cavity. Iron (II) is oxidised within the ferroxidase centers located at the entrance of ferritin pores (threefold channels on the protein surface) and subsequently transferred to the central cavity and mineralised as iron (III) oxide nanocrystals. Thereafter, under physiological reducing conditions, the iron (III) oxide can be reverted to iron (II) and diffuses out of the cavity, most likely through negatively charged pores in the ferritin shell, formed between subunits [1]. These channels allow for the entry and exit of cations during mineralisation and demineralisation and display a relatively broad selectivity thus allowing for the accumulation of a variety of metal ions, with a preference for divalent cations. These properties have been used to develop ferritin as a drug delivery platform [2]. At physiological pH ferritin exists as a stable 24-mer, whereas in highly acidic or basic solutions it disassembles reversibly thereby spontaneously reassembling as neutral pH is restored. The reversible subunit assembly has been used to trap molecules in solution within its cavity simply by changing pH in the presence of the desired molecule. This property has been used to load the cavity with metal containing drugs, such as the cancer drug cisplatin [3, 4], and the iron chelator desferrioxamine B [5, 6], as well as a variety of organic and inorganic compounds, including metal nanoparticles.

The incorporation of non-metal-containing drugs within ferritin is however challenging due to the limited interactions with the ferritin shell, and the diffusion of these molecules through the surface pores. Strategies to overcome these problems have focused on complexing drugs with transition metals, such as Cu(II), prior to their internalisation [7], or the addition of charged accessory molecules such as poly-L-aspartic acid to optimise loading of ferritin with drugs [8]. By combining the loading of ferritin with drugs and surface modification with peptide epitopes and labels, ferritin can be specifically targeted to particular cell types and tumours for efficient delivery of therapeutic agents [9]. Thus far, ferritins and other protein nanocages show a great deal of promise that will hopefully transfer to a clinical setting.

Nevertheless, molecular diffusion in and out of the ferritin cavity appears to be a complex phenomenon that is only partially understood. The pathway of iron entry inside the ferritin cavity is

characterized by the presence of eight protein ion channels positioned around the threefold symmetry axes of the cage and delimited by three proximal subunits. Such ion channels are about 15 Å in length and 5–6 Å in diameter. Because hydrated ions have diameters of about 6.5 Å, partial dehydration is thought to occur for ion passage through the channel. On this basis, possible entry of larger ligands of physiological interest (e.g. iron III reductants) or other small organic molecules may seem unlikely. However, a large number of experimental observations, mostly carried out on mammalian ferritins heteropolimers or recombinant H and L homopolimers, pointed out that small organic molecules can permeate the protein shell, possibly through the same negatively charged threefold channels that govern metal ions fluxes [10, 11, 12]. The permeation of small molecules into ferritins at physiological temperature and pH has been shown to be a charge-selective process in both native, H and L-chains of several mammalian proteins having similar channel structures [13]. A number of studies thus supported the hypothesis that the threefold channels are indeed the primary avenues of entry into the protein cavity of small molecules endowed with cationic properties [14]. The complete exclusion of the negatively charged probes from the interior of these proteins has been elegantly demonstrated by means of spin labeled molecules [11]. At the same time, the permeability of the same molecules in mutated proteins bearing positively charged groups along the three fold channels has been demonstrated [15, 16]. More recently, however, many different ferritins from phylogenetically distinct trees have been identified and characterized. Among these, highly thermostable ferritins from Archaea emerged as privileged scaffolds in view of their remarkable thermal stability, easy expression in high yields in common *E. coli* cells and, at least in a few examples, uncommon association-dissociation properties. In particular, archaeal ferritins from *Archaeoglobus fulgidus* (Af-Ft) and *Pyrococcus furiosus* (Pf-Ft) emerged as most interesting tools for diverse applications. In spite of the high sequence similarity (50 and 70% amino acid sequence identity and similarity, respectively), Pf-Ft and Af-Ft do not share the same quaternary assembly. In fact, whereas the Pf-Ft 24-mer has the canonical 432 point-group symmetry, the Af-Ft 24-mer displays a 23 point-group symmetry typical of smaller 12-mer ferritin-like proteins. This unusual assembly does not display the 4-fold channels and constrains the quaternary structure thus leading to the appearance of four large triangular openings about 45 Å wide in the protein shell [17]. To date, Af-Ft assembly, here referred to as an “open” structure, is considered unique among all other known structures of tetraeicosameric ferritins. The stability of this tetrahedral configuration is governed by two critical residues in the helix E of the 4-helices bundle, namely K150 and R151. Indeed, the structure of Af-Ft K150A/R151A mutant reported by Sana et al. [18], shows a typical “closed” octahedral symmetry.

However, diffusion of small molecules within archaeal ferritins have been little investigated. Differences in the nature, shape and properties of open pores within these ferritins thus provide novel possible routes for small molecules entry/incorporation thus expanding the scope of possible biotechnological applications of these proteins. In the present work, we have engineered a set of Pf-Ft, Af-Ft ("open") and Af-Ft K150A/R151A ("closed") mutants by placing reactive cysteine residues in the same topological positions either inside or outside the internal cavity. The reactivity of the bulky, negatively charged DTNB molecule has been probed in the set of available mutants.

2. Materials and methods

2.1 Point mutations and protein expression

The genes encoding for bacterial ferritin from Af-Ft and Pf-Ft were cloned into the expression vector pET22b (Novagen). Point mutants Af-FtM54C, Af-FtM54C/K150A/R151A, Pf-FtG52C and Pf-FtP77C were obtained by PCR using QuickChange Mutagenesis kit (Stratagene). The recombinant plasmids were transformed into *E. coli* TOP 10 cells and the resulting colonies were screened by DNA sequencing. Plasmids bearing the desired mutations were transformed into BL21(DE3) *E. coli* strain for protein expression. For each mutant, protein over-expression was obtained as follows: 1 L LB broth medium was inoculated with 2 ml overnight culture of a single colony and the gene expression was induced with 1 mM IPTG when the absorbance at 600 nm reached 0.6. Cells were harvested by centrifugation after overnight induction at 37 °C and the cell pellets were stored at -20°C.

2.2 Protein purification

Harvested cells form 1 L colture over-expressing Af-FtM54C and Af-FtM54C/K150A/R151A mutants were resuspended in 20 ml buffer A (25 mM HEPES pH 7.5, 20 mM $MgCl_2$) containing a cOmplete™ Mini Protease Inhibitor Cocktail Tablet (Roche) and disrupted by sonication. The soluble fraction was thermally purified by heating at 85 °C for 10 minutes followed by removal of denatured proteins by centrifugation at 14000 rpm for 30 minutes at 4 °C. The supernatant was fractioned by ammonium sulfate precipitation. 70% ammonium sulfate pellet containing highly purified protein was resuspended in buffer A, dialysed versus the same buffer, sterile filtered and stored at 4°C. Cells over-expressing Pf-FtG52C and Pf-FtP77C were sonicated in 25 mM HEPES buffer at pH 7.5 containing 0.5 mM EDTA, 0.3 M NaCl and cOmplete™ Mini Protease Inhibitor Cocktail Tablet. After sonication, the crude bacterial extract was digested with DNase for 1 hour at 37 °C, heated at 55 °C for 10 minutes and then at 80 °C for 8 minutes. Heat treatment was followed by centrifugation to remove insoluble material and ammonium sulfate pre-

cipitation. 70% ammonium sulfate pellet was resupended in 20 mM HEPES pH 7.5 plus 150 mM NaCl, dialysed versus the same buffer and loaded onto a HiLoad 26/600 Superdex 200 pg column (GE Healthcare). Fractions containing highly purified protein were pooled, sterile filtered and store at 4 °C.

2.3 Preparation of Ferritin-DTNB adducts

All mutants were reduced with 3 mM TCEP (tris(2-carboxyethyl)phosphine) in their storage buffers and then loaded onto a desalting column (GE Healthcare) to remove the reducing agent. Each mutant was reacted with 40-fold molar excess of Ellman's Reagent, (DTNB) per cysteine for 3 hours at room temperature. Stock DTNB solutions were prepared in ethanol. The excess (non-reacted) reagent was removed by ultra-filtration using 100 kDa Amicon Ultra-15 centrifugal devices (Millipore Corporate). The Ferritin–DTNB samples were analyzed by mass spectrometry as described below.

2.4 Stopped flow experiments

Kinetic measurements were carried out on a thermostated Applied Photophysics stopped-flow apparatus (Leatherhead, UK) by mixing 8-10 μM protein solutions, previously reduced with TCEP, with solutions containing different concentrations of DTNB (from 0.2 to 0.7 mM after mixing) in 20 mM HEPES, 20 mM $MgCl_2$ pH 7.5. In order to avoid interference of the instrument phototube from the high concentrations of DTNB and the released chromophore 5-thio-2-nitro-benzoic acid (TNB), the reaction was followed at 430 nm and the extinction coefficient calculated to be 12205 $mM^{-1}cm^{-1}$, as determined from the extinction coefficient of 14150 $mM^{-1}cm^{-1}$ at 412 nm [19]. All fitting procedures were carried out by using the Matlab software (Mathworks, USA). Experimental traces were fitted by non-linear regression to either exponential of biexponential processes by using an Levenberg-Marquardt algorithm.

2.5 Self-assembly study

$MgCl_2$ -mediated self-assembly of ferritin mutants was studied by incubating aliquots of proteins (1 mg/ml) with different salt concentrations in 25 mM HEPES buffer, pH 7.5. Molecular sizes of Af-FtM54C, Af-FtM54C/K150A/R151A, Pf-FtG52C and Pf-FtP77C was determined by size exclusion chromatography (SEC) using HiPrep 16/60 Sephacryl S300 column (GE Healthcare). The column was equilibrated with 25 mM HEPES, pH 7.5, containing $MgCl_2$ at the same concentration in which the protein was pre-incubated and the same buffer was used as mobile phase. Mo-

lecular weight of each mutant were determined by comparing their elution volumes with the elution volumes of standard proteins in the same salt concentration.

Dynamic light scattering measurements (DLS) were performed using an ALV-5000 logarithmic correlator in combination with a standard optical set-up based on a He–Ne (λ = 632.8 nm) 10 mW laser and a photomultiplier detector. The intensity autocorrelation functions were directly obtained as $g_2(q, t) = \langle I(q, t)I(q, 0)\rangle / \langle I(q, 0)\rangle^2$, where q is the modulus of the scattering vector defined as $q = (4\pi n/\lambda) \sin(\theta/2)$ ($\theta = 90^\circ$ in the present experiment). The raw measurements as directly obtained, without any data corrections are shown in Fig. 1 for different samples without added salt (black symbols) and at different $MgCl_2$ concentrations between 5 and 30 mM (colored symbols as described in the legend. Quantitative analysis of the measurements was obtained through a fit of the data with a single exponential expression: $g_2(q, t)=1+be^{-t/\tau}$ where b is the coherence factor and τ is the relaxation time related to the motion of the particles, specifically to the diffusion coefficient [20]

2.6 Protein LC–MS

LC–MS was performed on protein samples before and after DTNB titration, after dialysis in distilled water in the presence of 0.1 mM EDTA, using a Waters AcquityuPLC connected to Waters Acquity Single Quad Detector. A Hypersil Gold C4 column was used: 1.9 μm, 2.1 × 50 mm at 254 nm observation wavelength; mobile phase: 95:5 water (0.1% formic acid):MeCN (0.1% formic acid); gradient over 6 min (to 5:75 water (0.1% formic acid):MeCN (0.1% formic acid); flow rate: 0.4 ml min^{-1}; MS mode was set at a scan range: m/z=250–2,000 (ES+); scan time: 0.25 s. Data were obtained in continuum mode by setting the electrospray source of the MS with a capillary voltage of 3.5 kV and a cone voltage of 50 V. N_2 gas was used as nebulizer and desolvation gas at a total flow of 300 l/hours. Ion series were generated by integration of the ultraviolet-absorbance (at 254 nm) chromatogram over 1.2–1.8 min range. Mass spectra were subsequently reconstructed for proteins from the ion series using the MaxEnt 1 algorithm on MassLynx software program.

3. Results

3.1 Assessment of ferritin mutants assembly.

In order to assess the association state of the engineered ferritin mutants Af-FtM54C, Af-FtM54C/K150A/R151A, Pf-FtG52C and Pf-FtP77C, all proteins were studied by DLS and SEC as a function of $MgCl_2$ concentration. A full characterization of Af-FtM54C association state is reported in Figure 1. Data relative to the other mutants are reported as Supplementary Materials (Figures S1, S2 and S3). Figure 1 clearly shows that the shape of the curve without added salt is significantly

different from that observed in the presence of added salt. This behavior is confirmed by data fitting obtained as described under Methods section. The fitting curves appears to interpolate very well experimental data in presence of salts whereas are less accurate for samples without added salt, where the addition of polydispersity is necessary.

Pf-Ft mutants are stable 24-mers (~490 kDa) independent of salt concentration, whereas the self-assembly of Af-Ft mutants was strongly dependent on ionic strength. $MgCl_2$ was used as polymerizing salt at variance with previous reports [18] in which NaCl was used. As a result, it appeared that at our working concentration (20 mM $MgCl_2$) all the proteins are structured as a stable 24-meric cage. It is noticeable that the 24-mer to dimer ratio increases with increasing $MgCl_2$ concentration from 0 to 20 mM, whereas at least 100 mM NaCl concentration of NaCl are needed to reach full polymerization (data not shown). Thus, it appears that divalent cations such as Mg^{2+} and Ca^{2+} are more effective in promoting the 24-mer association with respect to NaCl. The comparison between SEC and DLS data on Af-FtM54C and Af-FtM54C/K150A/R151A however need further comments. First of all, the heterogeneous, polydisperse population observed in the absence of divalent cations is manifest in the presence of both low molecular weight species (presumably dimers as reported in refs. 16-18) and distributed high molecular weight polymers (present in much lower amount), apparently in a proportion even higher than the canonical 24-mers. Addition of $MgCl_2$ at 5-10 mM concentration brings about a very sharp transition in both Af-Ft mutants resulting in the formation of homogeneous and stable 24-mer species. At 20 mM $MgCl_2$ concentration, all proteins investigated are consistent with a stable 24-mer assembly.

3.2 Kinetics of DTNB binding to Pf-Ft and Af-Ft mutants.

The kinetics of the disulfide exchange reaction of DTNB with cysteine residues on ferritin mutants were carried out by stopped-flow spectroscopy. The kinetics, determined under pseudo-first order conditions, appeared to be multiexponential and were followed to the maximum time possible with the instrument (1000 s). Independent experiments performed by using UV-visible absorption spectroscopy and LC-MS (see below) confirmed the essentially complete cysteine reactivity. As Fig. 2 A shows, the time scales of the four ferritin mutants are significantly different. As expected, the Pf-Ft P77C mutant bearing the cysteine residue on the convex outer surface displayed the fastest reactivity as compared to Pf-Ft G52C which carries the mutation inside the ferritin tetraeicosamer. A complete set of time courses of the Pf-Ft P77C mutant has been carried out increasing DTNB concentration and reported in Supplementary Materials (Fig. S4). Within the observed time frame all traces could be fit to a simple relaxation process with apparent second-order rate constants of *ca*. 900 $M^{-1}cm^{-1}$ (see also Table 1). The Af-Ft mutants had an intermediate behaviour in the reaction

with DTNB. Quite unexpectedly the Af-Ft M54C mutant, in which the internal cysteine reacts with DTNB in a facilitated way through the four 45-Å large triangular openings in the protein shell, could only be fit by a biexponential process in which the fastest second-order rate constant was of the same order of magnitude determined for the Pf-Ft P77C mutant (Table 1). Finally, closure of the openings by introduction of the K150A/R151A mutations in Af-M54C brought about a significant quenching of the ligand binding rate. The complete set of kinetic traces for each mutant were also fit by either exponential or biexponential relaxations with second-order rate constants as reported in Supplementary Materials (Fig. S5). Overall these results indicate that the diffusion of molecules across the proteinaceous barrier of closed ferritin 24-mers can be accurately measured and secondly that contrary to intuition and reported data (see discussion section) the protein shell permeability to bulky molecules such as DTNB is much higher than expected. These results bear relevant implications discussed below in so far as ligand encapsulation and delivery is concerned.

3.3 LC/MS data

LC–MS measurements were performed on the selected point mutants Af-FtM54C, Af-FtM54C/K150A/R151A, Pf-FtG52C and Pf-FtP77C after titration with DTNB in comparison with unreacted proteins. In all samples, ferritins were eluted as monomers of molecular weight of about 21 kDa, and DTNB reacted proteins showed a shifted peak of +198 ± 2 Dalton, in agreement with the expected molecular weight of the thio-nitrobenzoic moiety. In all samples reaction was complete with the exception of Pf-Ft G52C protein in which 18 % of unreacted protein was present (Supplementary Materials, Fig. S6).

4. Discussion

The present data highlight notable properties related to bulky ligands penetration through prototypic archaeal ferritin homopolymers that are relevant both to the general ligand entry/escape mechanism and to the widespread nanotechnological applications of these proteins [21, 22].

The experimental set up was designed around four mutants of Pf-Ft and Af-Ft bearing a cysteine residue per subunit either in topologically equivalent positions inside the 24-mer cavity (Af-FtM54C, Af-FtM54C/K150A/R151A, Pf-FtG52C) or outside the 24-mer cage in the Pf-FtP77C mutant (see Fig. 3). In this framework, access to the reactive sulfidryls is totally unhindered on the protein external surface in Pf-FtP77C, partially hindered in the internal cavity in Af-FtM54C and totally hindered in the internal cavity in Af-FtM54C/K150A/R151A and Pf-FtG52C. The overall picture that emerges from the body of experimental results is that even fully assembled, closed Af-FtM54C/K150A/R151A and Pf-FtG52C structures are capable of stoichiometric binding of the

bulky, negatively charged, DTNB ligand. These results indicate that the permeation of negatively charged molecular species of 8–10 Å length and 5-6 Å diameter into archaeal ferritins does occur at variance with the reported exclusive entry of positively charged or neutral species only in vertebrate ferritins [13, 14]. Charge selectivity was reported in the case of horse spleen ferritin (HoSF) and human H-chain ferritin (HuHF) and was correlated to the nature of threefold channels, endowed with hydrophilic, negatively charged tunnels involved in iron uptake [23]. Electron paramagnetic resonance spectroscopy and gel permeation chromatography studies with HoSF demonstrated that molecular charge and polarity of the diffusants play a critical role in their permeation into ferritin [14]. Kinetic studies of permeation using small nitroxide spin probes also confirmed the role of these channels as providing a charge-selective pathway for entry into the cavity [10]. A negatively charged nitroxide was completely excluded from the interior of the protein, whereas positively charged and polar nitroxide radicals penetrated the protein shell to interact with the iron core. Mutated HuHF (D131H/E134H), where the negatively charged glutamate and aspartate residues lining the threefold channels are replaced by histidines, partially allowed the entry of negatively charged species (4-carboxyTEMPO radical) thus providing strong evidence that the negatively charged threefold channels are the principal pathways for molecular diffusion into ferritin [10]. Interestingly, first-order half-lives for permeation of positively charged compounds in mammalian ferritins are in the same time range of those observed in DTNB uptake in fully closed Af-FtM54C/K150A/R151A and Pf-FtG52C archaeal ferritins although Af-Ft and Pf-Ft have been reported to show a different amino acid arrangement in the threefold channels that suggested a different ligand incorporation mechanism.

In particular, the eight threefold channels in each protein are shaped by the C-terminal segment of C helix and the N-terminus of D helix in the 4-helix bundle of three adjacent monomers [24]. Thus, C-terminal ends of helices C define the outer entrance to the channel and the N-termini of helices D define the inner entrance. In the case of Pf-Ft, channels are similar to those of HuHF in the outer side, that is rich in negative aminoacids (Glu109, Glu110 and Glu111), whereas they differ in the central region due to the presence of polar and positively charged residues (Tyr114 and Arg117). Lastly, the inner entrance of the channel is characterized by the presence of Ala118 and Glu121, in the topological position which is deemed essential for the transfer of iron (II) to the ferroxidasic center in mammalian ferritins [26].

In the case of Af-Fts, namely Af-FtM54C (“open” form) and Af-FtM54C/K150A/R151A (“closed” form), the threefold channels are lined by a mix of hydrophobic and hydrophilic aminoacids: only one glutamate (Glu113; PBD ID: 1SQ3 and 3KX9) is located to the entrance and two acidic residues lining HuHF channels (D131 and E134) (PDB ID:2FHA) are replaced by neu-

tral and positively charged residues (Tyr119 and Asn 120). Thus, in the case of Af-Ft, the cluster of negative charges characteristic of HuHF is not present, presumably because it is not necessary to drive iron (II) atoms towards the ferroxidasic site, readily available through the large pores present in this protein. Hence, the threefold channels of archaeal ferritins are less negatively charged than the mammalian ones, possibly allowing the entrance of negatively charged compounds (see Fig. 4). Of course, the "open" Af-FtM54C, here investigated, displays the four 45 Å wide triangular pores, defined by C and D helices, characterized by the presence of a group of positive charged residues located at the three apices [17]. These large openings are most likely preferential paths for large ligand entry into the cavity as demonstrated by the 8 fold faster DTNB reaction rate with the internal thiol with respect to the closed Af-FtM54C/K150A/R151A mutant (see Table 1). In turn, the DTNB entry rate into Af-FtM54C/K150A/R151A mutant is 5 fold faster than in the Pf-FtG52C protein. Such difference is significant in view of the fact that the last two proteins are assimilated to closed cages with thiols in topologically equivalent positions.

As a last comment it is worth considering the possible role of the so-called fourfold channels. As matter of fact, the quaternary assembly of the closed Af-FtM54C/K150A/R151A mutant is similar to that of Pf-FtG52C and other mammalian Ft cages displaying a canonical octahedral conformation with fourfold channels of 4-5 Å size. The six fourfold channels of Pf-Ft (PDB ID: 2JD6) are polar and hydrophilic. Moreover, Lys145 in the DE loop (corresponding to Lys 150 in Af-Ft), which forms an outer gate to the fourfold channel, makes this entrance more polar and charged than that of HuHF, which is basically uncharged. Neverthless, the dimensions of the fourfold channel in both mammalian and archaeal ferritins is found to be too small even to metal ions with the possible exception of protons and cannot be taken as a possible option for the entry of organic molecules.

Thus, on the basis of the observed DTNB binding rates and available crystallographic structures we conclude that archaeal ferritins from *P. furiosus* and *A. fulgidus* are able to incorporate negatively charged, modestly sized diffusants, even in their fully "closed" forms, most likely through the threefold channels whose nature appears less restrictive with respect to that of vertebrate proteins. Possibly, the presence of positively charged residues in the middle of the threefold channel may favour entrance of negatively charged species in the archaeal proteins. As a last comment, it must also be pointed out that the dimensions of the currently used probe slightly exceed the diameter of the threefold channel as inferred from crystal structure coordinates. A mechanism of rotameric adjustment of relevant aminoacid side chains is thus necessary in order to allow for the entry/exit of small organic molecules. Recent demonstration of multiple conformers in aminoacids lining the inner entrance to the ferritin cavity may explain the necessary plasticity of the threefold channels in ferritins [26].

6. Conclusions

The results of the present work indicate that molecular diffusion into archaeal ferritin is a complex phenomenon and that even apparently closed, impermeable structures, ferritins do allow entry of 8-10 Å long organic molecules with no necessity of 24-mer desassembly. The data thus obtained indicate clearly that the protein matrix in archaeal ferritins does not provide a significant barrier against bulky, negatively charged ligands such as DTNB, a finding of relevance in view of the multiple biotechnological applications of these ferritins that envisage ligand encapsulation within the internal cavity. The potential impact of such engineered ferritins on the general topics related to their biotechnological application is wide. On the side of material science, the possibility of disposing of a cations dependent self-assembling cage provides the basis of unique "molecular carpentry" tools. On the side of biomedical applications, the use of archaeal proteins must still be explored. The entry of archaeal ferritins into mammalian cells is under investigation in order to clarify their receptor recognition properties, the pathways of intracellular trafficking, the impact on eukaryotic cell iron homeostasis and/or their toxic effects due to possible generation of oxidative stress under the widely different iron reductive mechanisms typical of eukaryotic cells.

Acknowledgements

EU H_{2020} Project "X-Probe", Grant N° 637295, to A. Bonamore and M.C.T. is gratefully acknowledged. Flagship project "Nanomax" from MIUR to A. Boffi is also acknowledged.

References

[1] K. Honarmand Ebrahimi, P.L. Hagedoorn, W.R. Hagen, Unity in the biochemistry of the iron-storage proteins ferritin and bacterioferritin, Chem. Rev. 115 (2015) 295-326.
[2] Z. Zhen, W. Tang, H. Chen, X. Lin, T. Todd, G. Wang, RGD-modified apoferritin nanoparticles for efficient drug delivery to tumors, ACS Nano 7 (2013) 4830–4837.
[3] N. Pontillo, F. Pane, L. Messori, A. Amoresano, A. Merlino, Cisplatin encapsulation within a ferritin nanocage: a high-resolution crystallographic study, Chem. Commun. (Camb) 52 (2016), 4136-4139.
[4] E. Falvo, E. Tremante, R. Fraioli, C. Leonetti, C. Zamparelli, A. Boffi, V. Morea, P. Ceci, P. Giacomini, Antibody-drug conjugates: targeting melanoma with cisplatin encapsulated in protein-cage nanoparticles based on human ferritin, Nanoscale 5 (2013) 12278-12285.
[5] X.-T. Ji, L. Huang, H.-Q. Huang, Construction of nanometer cisplatin core-ferritin (NCC-F) and proteomic analysis of gastric cancer cell apoptosis induced with cisplatin released from the NCC-F, J. Proteomics 75 (2012), 3145–3157.
[6] J.M. Domínguez-Vera, Iron(III) complexation of Desferrioxamine B encapsulated in apoferritin, J. Inorg. Biochem. 98 (2004), 469–472.
[7] A. Maham, Z. Tang, H. Wu, J. Wang, Y. Lin Protein-based nanomedicine platforms for drug delivery, Small, 5 (2009), 1706–1721.
[8] A. Maham, H. Wu, J. Wang, X. Kang, Y. Zhang, Y. Lin, Apoferritin-based nanomedicine platform for drug delivery: equilibrium binding study of daunomycin with DNA, J. Mater. Chem. 21 (2011), 8700-8708.
[9] L. Vannucci, E. Falvo, C.M. Failla, M. Carbo, M. Fornara, R. Canese, S. Cecchetti, L. Rajsiglova, D. Stakheev, J. Krizan, A. Boffi, G. Carpinelli, V. Morea, P. Ceci, In Vivo Targeting of Cutaneous Melanoma Using a Melanoma Stimulating Hormone-Engineered Human Protein Cage with Fluorophore and Magnetic Resonance Imaging Tracers, J. Biomed. Nanotechnol. 11 (2015) 81-92.
[10] X. Yang, P. Arosio, N.D. Chasteen, Molecular diffusion into ferritin: pathways, temperature dependence, incubation time, and concentration effects, Biophys. J. 78 (2000) 2049-2059.
[11] X. Yang, N.D. Chasteen, Molecular diffusion into horse spleen ferritin: a nitroxide radical spin probe study, Biophys. J. 71 (1996) 1587-1595.
[12] B. Zhang, R.K. Watt, N. Gálvez, J.M. Domínguez-Vera, G.D. Watt, Rate of iron transfer through the horse spleen ferritin shell determined by the rate of formation of Prussian Blue and Fe-desferrioxamine within the ferritin cavity, Biophys. Chem. 120 (2006) 96-105.
[13] R.R. Crichton, J.P. Declercq, X-ray structures of ferritins and related proteins, Biochim. Biophys. Acta1800 (2010) 760-818.
[14] T. Douglas, D.R. Ripoll, Calculated electrostatic gradients in recombinant H-chain ferritin, Protein Sci. 1998 May;7(5):1083-91
[15] P.M. Harrison, A. Treffry, T.H. Lilley, Ferritin as an iron-storage protein: mechanisms of iron uptake, J. Inorg. Biochem.27 (1986) 287-293.
[16] A. Treffry, P.M. Harrison, Spectroscopic studies on the binding of iron, terbium, and zinc by apoferritin, J. Inorg. Biochem. 21 (1984) 9-20.
[17] E. Johnson, D. Cascio, M.R. Sawaya, M. Gingery, I. Schröder, Crystal structures of a tetrahedral open pore ferritin from the hyperthermophilic archaeon *Archaeoglobus fulgidus*, Structure 13 (2005) 637-648.
[18] B. Sana, E. Johnson, P. Le Magueres, A. Criswell, D. Cascio, S. Lim, The role of nonconserved residues of *Archaeoglobus fulgidus* ferritin on its unique structure and biophysical properties, J. Biol. Chem. 288 (2013) 32663-32672.
[19] P.W. Riddles, R.L. Blakeley, B. Zerner, Ellman's reagent: 5,5'-dithiobis(2-nitrobenzoic acid) -- a reexamination, Anal. Biochem. 94 (1979) 75-81.
[20] B.J. Berne, R. Pecora, Dynamic light scattering. Wiley, New York, 1976

[21] M. Liang, K. Fan, M. Zhou, D. Duan, J. Zheng, D. Yang, J. Feng, X. Yan, H-ferritin-nanocaged doxorubicin nanoparticles specifically target and kill tumors with a single-dose injection, Proc. Natl. Acad. Sci. USA111 (2014) 14900-14905.
[22] M.A. Kostiainen, P. Hiekkataipale, A. Laiho, V. Lemieux, J. Seitsonen, J. Ruokolainen, P. Ceci, Electrostatic assembly of binary nanoparticle superlattices using protein cages, Nat. Nanotechnol. 8 (2013) 52-56.
[23] A. Desideri, S. Stefanini, F. Polizio, R. Petruzzelli, E. Chiancone, Iron entry route in horse spleen apoferritin. Involvement of the three-fold channels as probed by selective reaction of cysteine-126 with the spin label 4-maleimido-tempo, FEBS Lett. 287 (1991) 10-14.
[24] J. Tatur, W.R. Hagen, P.M. Matias, Crystal structure of the ferritin from the hyperthermophilic archaeal anaerobe *Pyrococcus furiosus*, J. Biol. Inorg. Chem. 12 (2007) 615-630.
[25] E.F. Pettersen, T.D. Goddard, C.C. Huang, G.S. Couch, D.M. Greenblatt, E.C. Meng, T.E. Ferrin, UCSF Chimera--a visualization system for exploratory research and analysis, J. Comput. Chem. 25 (2004) 1605-1612.
[26] R.K. Beheraa, E.C. Theil, Moving Fe^{2+} from ferritin ion channels to catalytic OH centers depends on conserved protein cage carboxylates, Proc. Natl. Acad. Sci. U S A. 111 (2014) 7925–7930.

Figure legends

Fig. 1. Polymeric assembly of *Archaeoglobus fulgidus* ferritin mutants.
A) Dynamic Light Scattering intensity correlation functions of Af-FtM54C at different $MgCl_2$ concentrations indicated in the legend. The curves at different $MgCl_2$ are all superimposed.
B) Dynamic Light scattering relaxation time of Af-FtM54C as a function of $MgCl_2$ concentration.
C) Gel filtration profiles of Af-FtM54C at 20 mM $MgCl_2$

Fig. 2. Kinetics of DTNB binding to Af-Ft and Pf-Ft mutants. A. Comparison of the reaction time scales of all mutants; from left to right, Pf-FtP77C, Af-FtM54C, Af-FtM54C/K150A/R151A, and Pf-FtG52C. All mutants were 5 µM except Af-FtM54C which was 4 µM, and DTNB was 0.7 mM.

Fig. 3. Three-dimensional structures of the ferritin mutants. A monomer is depicted as green ribbon and the cysteine residues are represented in CPK style for clarity. a) Pf-FtP77C: the external cysteine is shown as blue spheres. b) Pf-FtC52C: the internal cysteine is depicted in red (models a) and b) built on Pf-Ft structure, PDB ID: 2JD6). c) Af-Ft54C: the internal cysteine is depicted in purple. d) Af-FtM54C/K150A/R151A: the internal cysteine in magenta (models c) and d) built on Af-Ft structure, (PDB ID: 1SQ3)). Molecular graphics and analyses were performed with the UCSF Chimera package [25].

Fig. 4. Profile view of the lining amino acids in the threefold channel in a) Af-Ft (PDB ID: 1SQ3) and b) Pf-Ft (PDB ID: 2JD6) with respect to c) HuHF (PDB ID: 2FHA). The exterior of the shell lies on the left side and the inner cavity on the right side of each cartoon as shown schematically. Positive, negative and polar residues are depicted as blue, red and green sticks, respectively.

Table 1. Apparent second-order constants for ferritin mutants as determined by the DTNB reaction.

Table

protein	*cysteine position*	k_{OBS} ($M^{-1}s^{-1}$)
Pf-FtP77C	external	908 ± 122
Pf-FtG52C	internal	5 ± 1
Af-FtM54C open	internal	fast: 198 ± 65 slow: 51 ± 21
Af-FtM54C/K150A/R151A closed	internal	26 ± 2

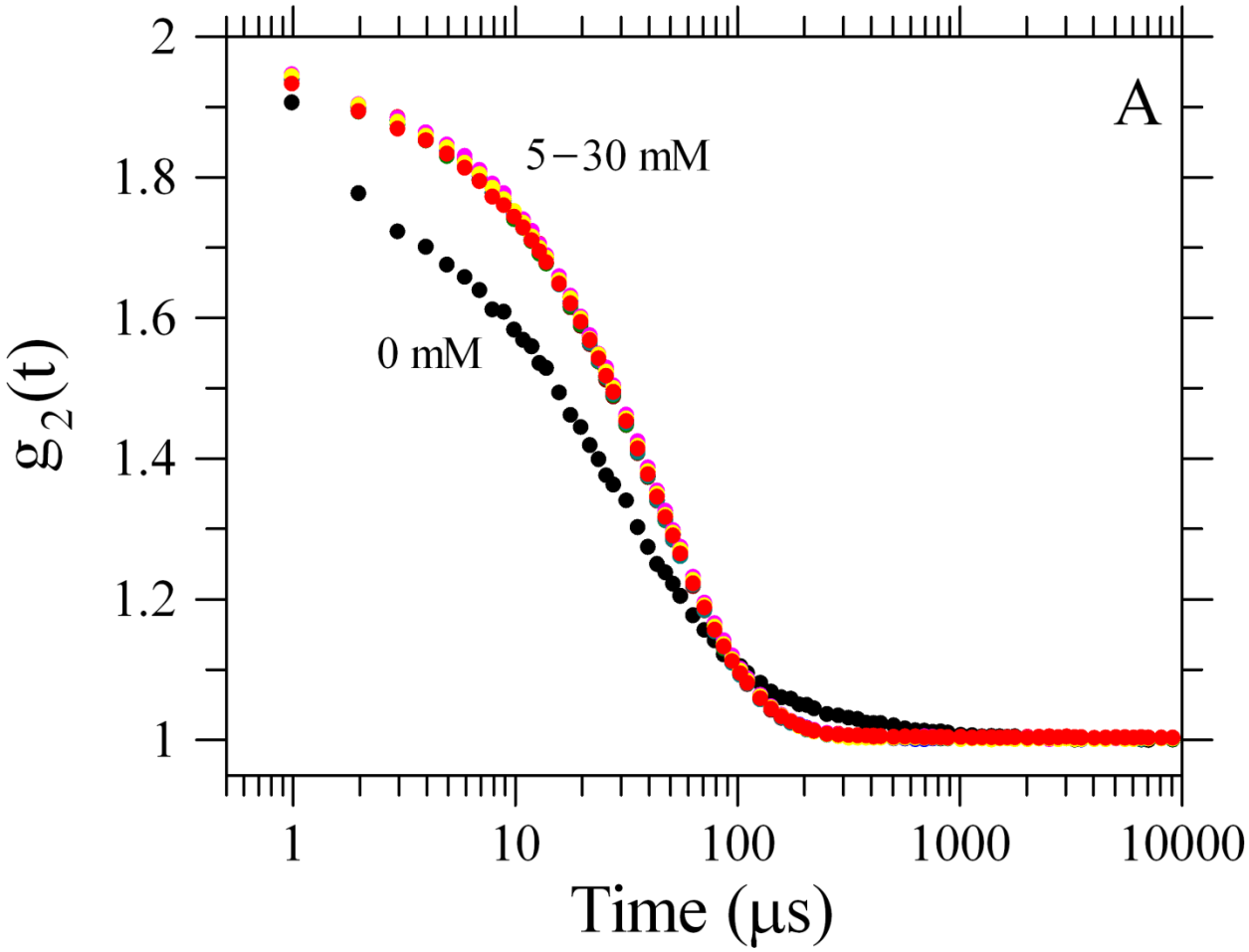

Fig. 1A

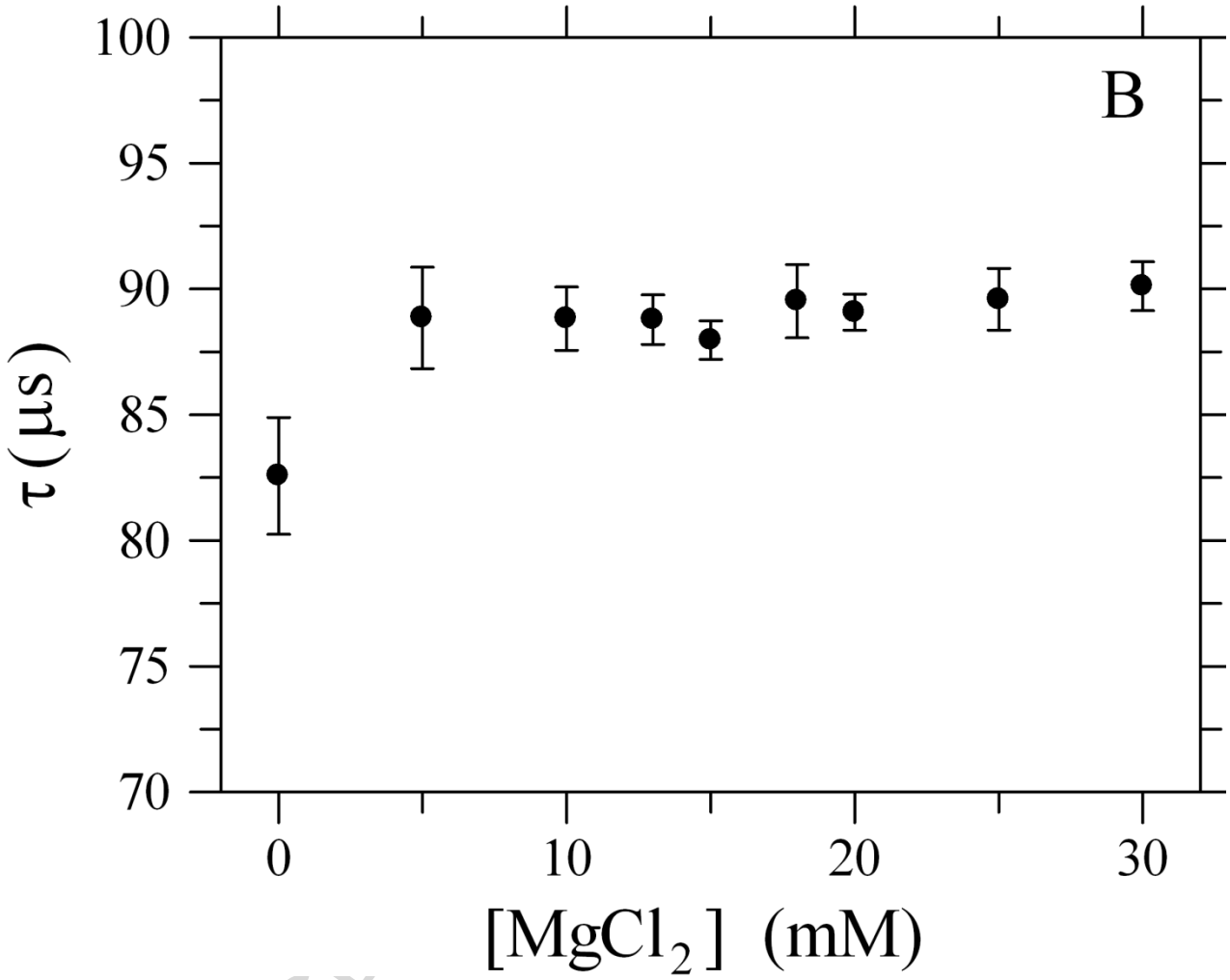

Fig. 1B

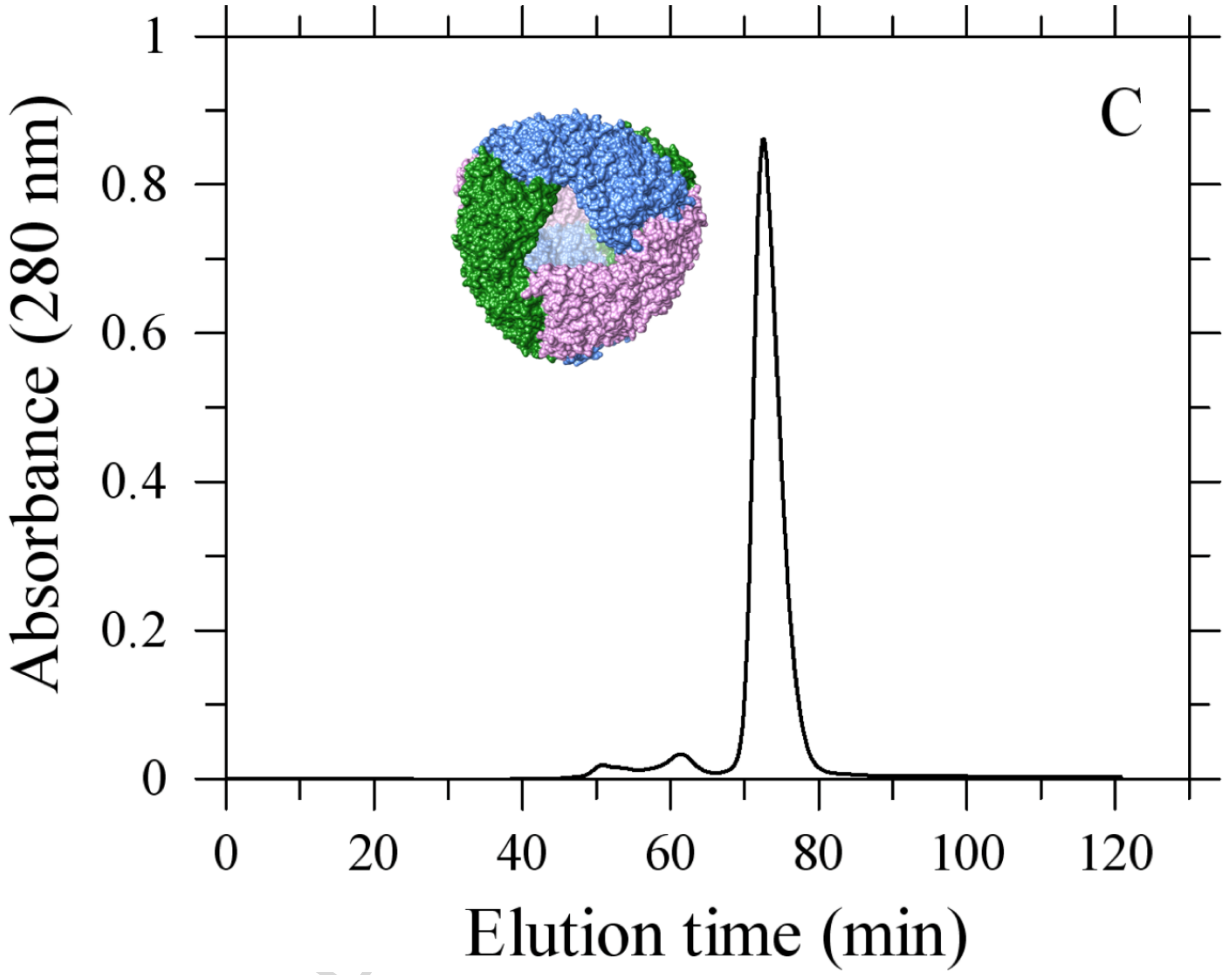

Fig. 1C

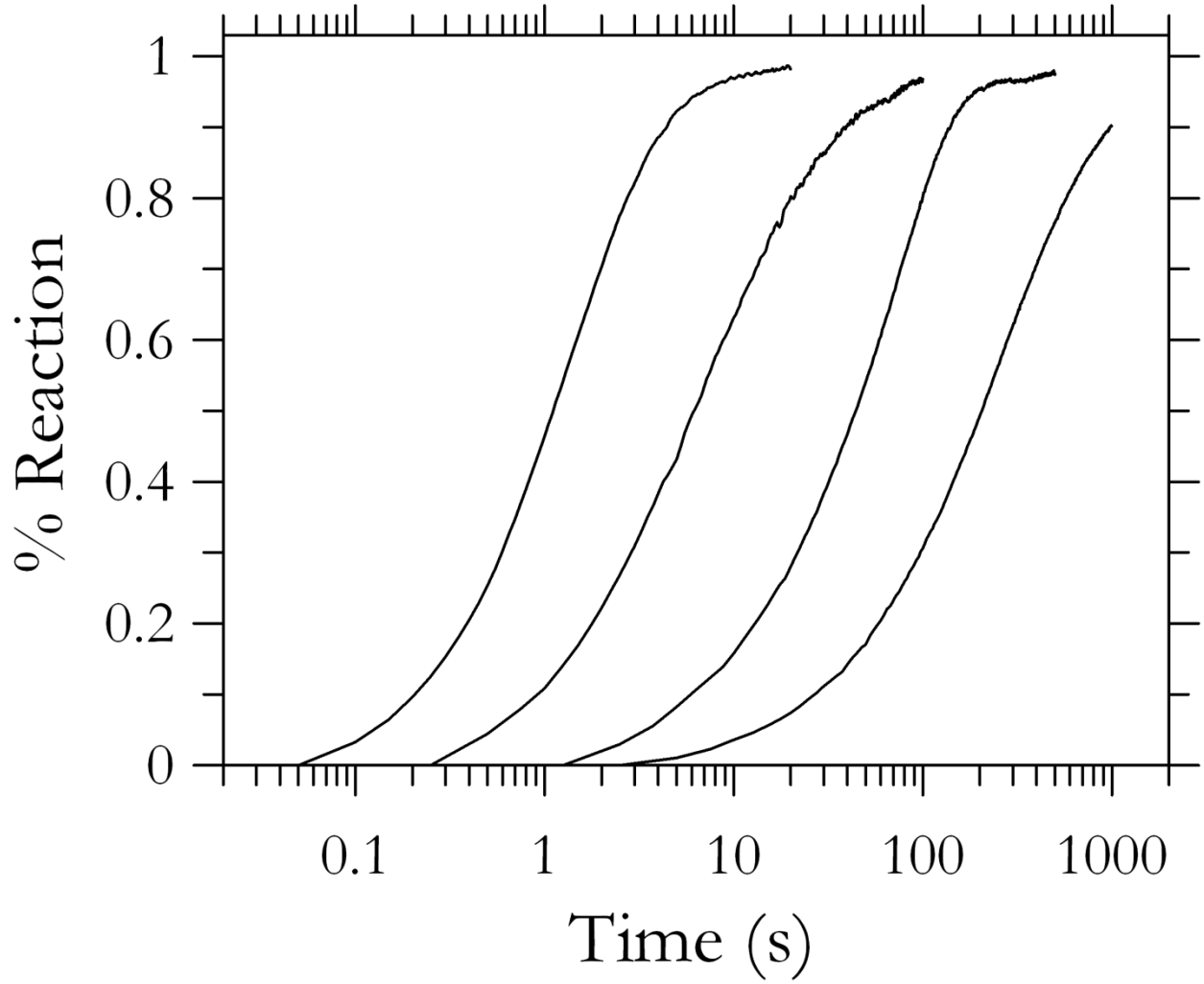

Fig. 2

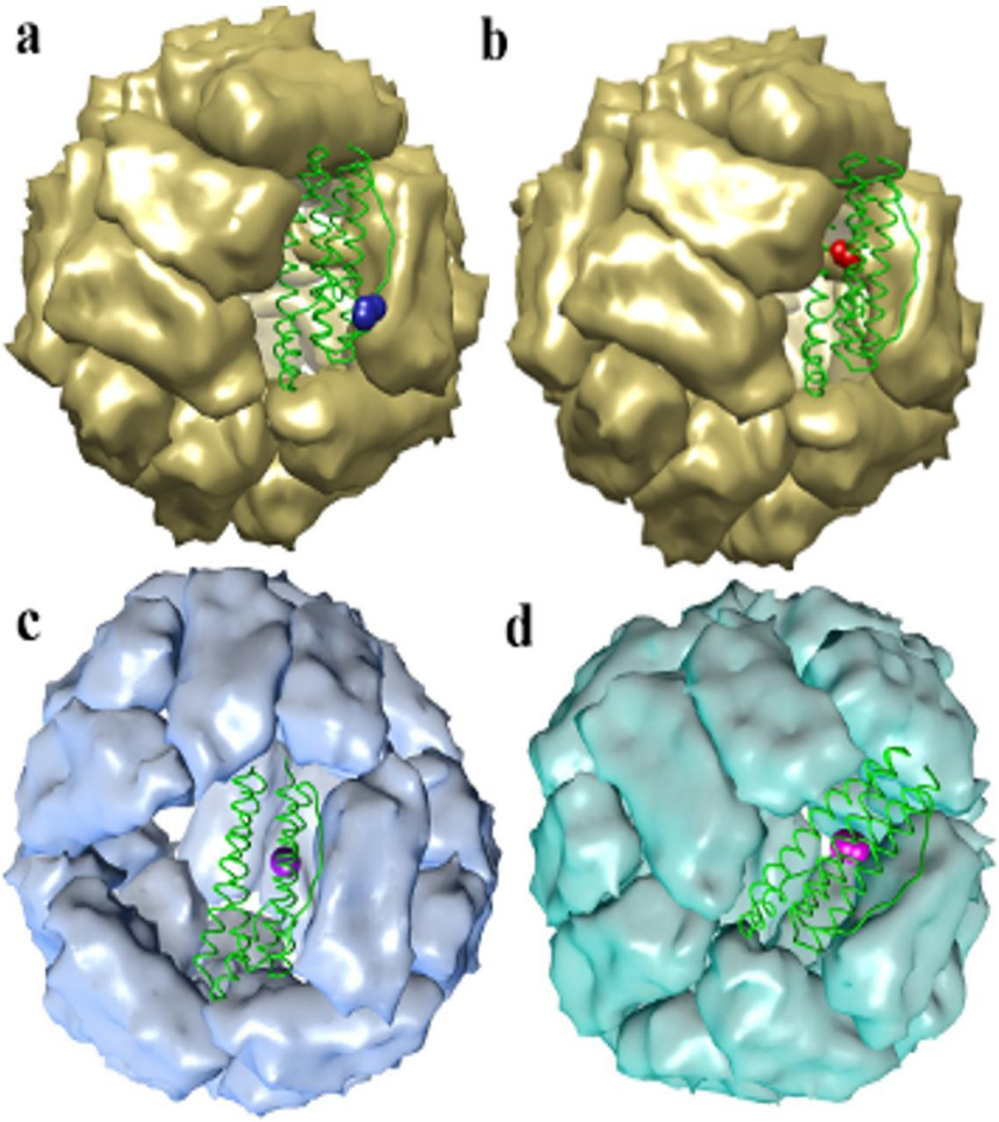

Fig. 3

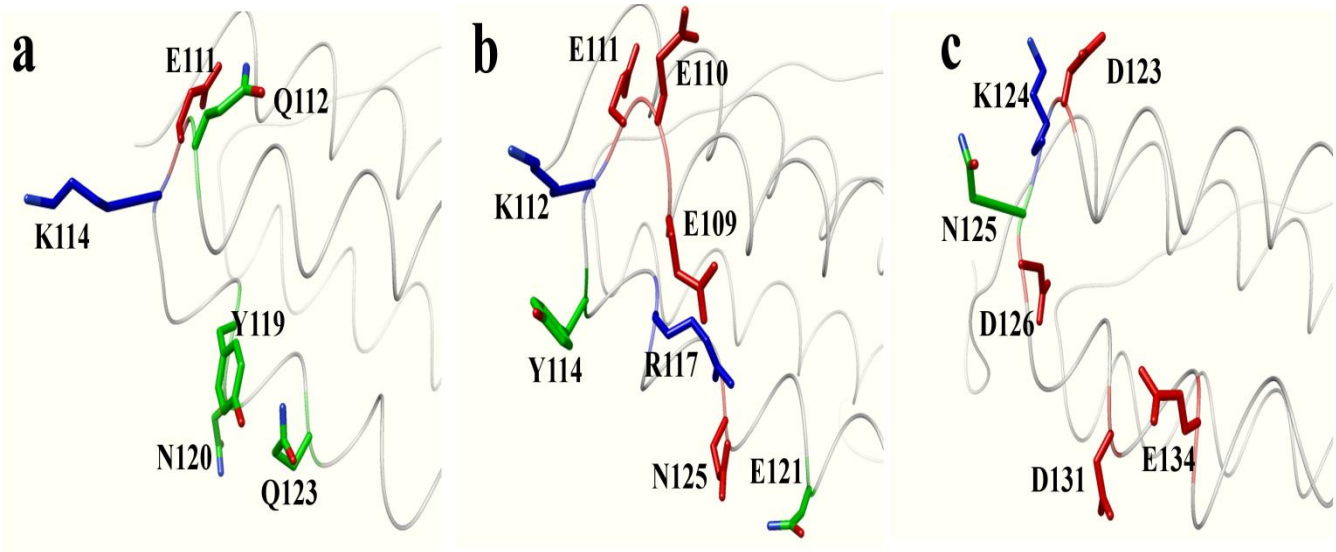

Fig. 4

Highlights

1) A set of engineered archael ferritin mutants have been obtained

2) The mutants bear cysteine thiols in selected topological positions

3) Thiol reactivity has been probed using the bulky thiol reactive DTNB

4) Archaeal ferritins can bind DTNB outside but also inside the cavity

5) Protein matrix is not a significant barrier against bulky, negatively charged ligands